Supporting Information

Brasier et al. 10.1073/pnas.1405338111

SI Text

SI Materials and Methods

A range of high-spatial-resolution techniques was used in this contribution. Both FIB-TEM and FIB-SEM were used to provide detailed morphological and chemical information on single slices through studied microstructures. In contrast, FIB-SEM 3D tomography was used to provide mostly morphological information from multiple slices that were then combined into 3D reconstructions of a given microstructure.

FIB Preparation of TEM Samples

Two dual-beam FIB systems (FEI xT Nova NanoLab 200 and FEI Helios Nanolab) located at the Electron Microscopy Unit (EMU), University of New South Wales, and at Adelaide Microscopy (AM), University of Adelaide, were used to prepare microfossil and pseudofossil TEM samples from standard uncovered polished geological thin sections coated with *ca*. 10 nm of gold. Electron beam imaging was used to identify microstructures of interest in the polished thin sections, allowing site-specific TEM samples to be prepared. The TEM sections were prepared by a series of steps involving different Ga^+ beam energies and currents (see ref. 1), resulting in ultrathin wafers of *ca*. 100 nm thickness. These TEM wafers were extracted using micromanipulators (in situ at AM; ex situ at EMU) and deposited on either continuous-carbon copper TEM grids, silicon TEM grids, or Omniprobe copper TEM sample holders. FIB preparation of TEM sections allows cell and cell-like features below the surface of the thin sections to be targeted, thus eliminating the risk of surface contamination. Note that FIB preparation of TEM samples destroys small adjacent portions of the microstructures of interest and therefore may not be applicable to unique samples.

TEM Analysis

TEM data were obtained using a JEOL 2100 LaB_6 TEM operating at 200 kV equipped with a Gatan Orius CCD camera and Tridiem energy filter, located in the Centre for Microscopy, Characterization and Analysis at The University of Western Australia. All elements (C, O, Mg, Al, Si, K, Fe, Ba) were identified using electron energy loss spectroscopy and mapped using the conventional three-window energy-filtered TEM technique (2), with energy windows selected to provide optimum signal-to-noise as follows: For carbon mapping, a 20-eV slit width was used centered on 249 eV (preedge 1), 269 eV (preedge 2), and 294 eV (postedge); for oxygen mapping, a 30-eV slit width centered on 484 eV (preedge 1), 514 eV (preedge 2), and 547 eV (postedge); for magnesium mapping, a 40-eV slit width was used centered on 1,240 eV (preedge 1), 1,280 eV (preedge 2), and 1,325 eV (postedge); for aluminum mapping, a 50-eV slit width was used centered on 1,480 eV (preedge 1), 1,530 eV (preedge 2), and 1,585 eV (postedge); for silicon mapping, a 60-eV slit width was used centered on 1,749 eV (preedge 1), 1,809 eV (preedge 2), and 1,874 eV (postedge); for potassium mapping, a 30-eV slit width was used centered on 244 eV (preedge 1), 274 eV (preedge 2), and 314 eV (postedge); for iron mapping, a 40-eV slit width was used centered on 638 eV (preedge 1), 678 eV (preedge 2), and 733 eV (postedge); and for barium mapping, a 30-eV slit width was used centered on 731 eV (preedge 1), 761 eV (preedge 2), and 801 eV (postedge). Elemental mapping was semiquantitative, and the detection limits are around 2 atomic %. Selected area electron diffraction for mineral identification was performed using an aperture that selected a *ca*. 200-nm-diameter area of the sample.

FIB-SEM and FIB-SEM 3D Nanotomography

FIB milling and SEM imaging was performed on a Zeiss Auriga Crossbeam dual-beam instrument at EMU and a FEI Helios Nanolab instrument at AM, following the methodology described in Wacey et al. (1). Milling and imaging parameters were optimized to suit the type of sample (i.e., carbon or pyrite within a silica or silicate matrix). Ga^+ ion beam currents of 1–2.8 nA were used for milling. Electron beams of 800 V to 5 kV were used for imaging with working distance tracked and tilt correction on. Sequential slices were milled with a slice spacing of 75–200 nm, depending on the size of the microstructure of interest, and each newly milled face was imaged with an image capture time of *ca*. 20–30 s. Semiquantitative elemental mapping of FIB-milled faces was performed using an Oxford X-Max SDD energy dispersive X-ray spectroscopy (EDS) system attached to the Zeiss Auriga Crossbeam instrument, with detection limits of about 0.5–1 atomic %. Note that FIB-SEM is destructive and may not be applicable to unique samples.

Three-Dimensional Volume Rendering

Sequential FIB-SEM nanotomography images were stacked, aligned, and cropped using SPIERSalign (3) or Image J. The resultant stacks were imported into SPIERSedit (3), where a number of masks were added to isolate individual components of the microfossil assemblages. The resulting files were exported and loaded into SPIERSview (3) to generate the 3D volume renderings. SPIERSview allows each individual masked component to be switched on or off, or made transparent, if necessary to better visualize adjacent components.

FIB-SEM nanotomography collects mostly morphological data. The pyritic and carbonaceous material studied here is easy to see in SEM images because of its different mass (hence contrast/brightness) compared with the silica matrix in which it is found. We routinely did EDS analysis on selected slices, to check that the pyritic and carbonaceous chemistry matched with the morphological features we saw, but did not do EDS on every slice, since that would have been far too time consuming. Hence, the 3D reconstructions do not depend on the size of a carbon or pyrite EDS peak. The 3D reconstructions are built primarily from morphological features visible in SEM, measured slice by slice.

For the carbonaceous examples of *Gunflintia* shown here, FIB-SEM 3D nanotomography provides evidence for lack of septation, for degradational holes in walls, and for wall modification by diagenetic silica growth (Fig. S2 *E* and *F*). For the pyritic examples of *Gunflintia* shown here, FIB-SEM 3D nanotomography provides evidence for tiny epiphytic cells clustering on *Gunflintia* filaments (Fig. S2 *C* and *D*). These are key observations that could not have been made in any other way in this study.

For the Strelley Pool material shown here, FIB-SEM 3D nanotomography confirms the spheroidal to ellipsoidal morphology of candidate microfossils (Fig. 5 *E*–*G*), suggests regions where cell walls may have been folded (Fig. 5*F*), and gives an indication of how much of the cell walls has been lost or replaced by diagenetic silica growth (Fig. 5 *E* and *G*). Once again, these are key observations that would be very difficult to achieve by any other technique (since FIB-SEM 3D nanotomography has better spatial resolution that other 3D techniques such as laser Raman or confocal laser scanning microscopy).

1. Wacey D, et al. (2012) Taphonomy of very ancient microfossils from the ~3400 Ma Strelley Pool Formation and ~1900 Ma Gunflint Formation: New insights using a focused ion beam. *Precambrian Res* 220-221:234–250.
2. Brydson R (2001) *Electron Energy Loss Spectroscopy* (Springer, New York), 160 pp.
3. Sutton MD, Garwood RJ, Siveter DJ, Siveter DJ (2012) SPIERS and VAXML: A software toolkit for tomographic visualization and a format for virtual specimen interchange. *Palaeontol Electron* 15(2):5T.

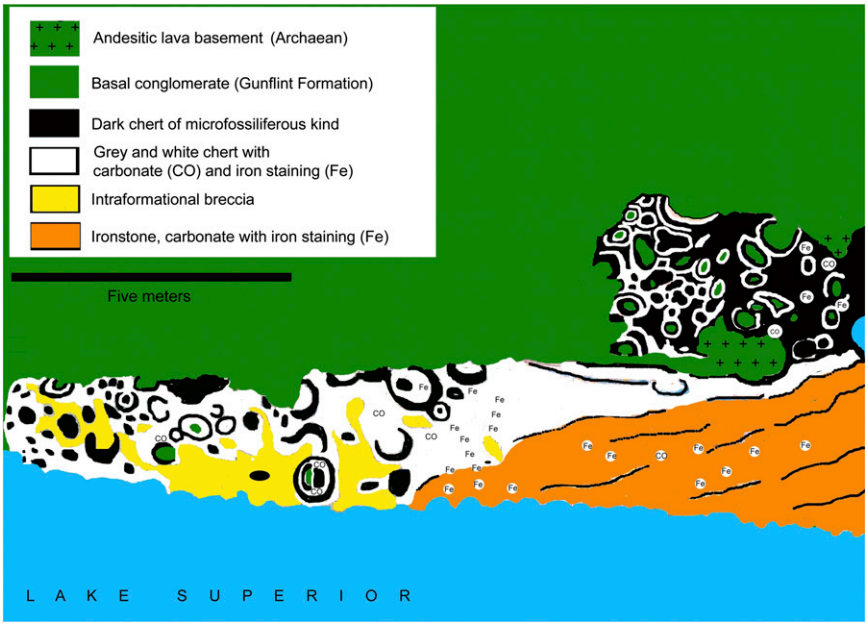

Fig. S1. Geological sketch map of the Schreiber Beach locality, exposed along the northern shore of Lake Superior, Ontario, Canada. This small outcrop provided the source for many of the well-preserved microfossils reported from the 1.88-Ga Gunflint chert (1). Such microfossils are typically found within carbonaceous and pyritic chert thin sections, derived from layers here marked in black. These layers formed episodically as microbial biolfims and early diagenetic mineral deposits accreted around the outside of large cobbles and boulders (of Archean lava) that became exposed along an ancient shoreline during the Paleoproterozoic (see *The Gunflint Chert: New Analytical Techniques*).

1. Barghoorn ES, Tyler SA (1965) Microorganisms from the Gunflint Chert. *Science* 147(3658):563–577.

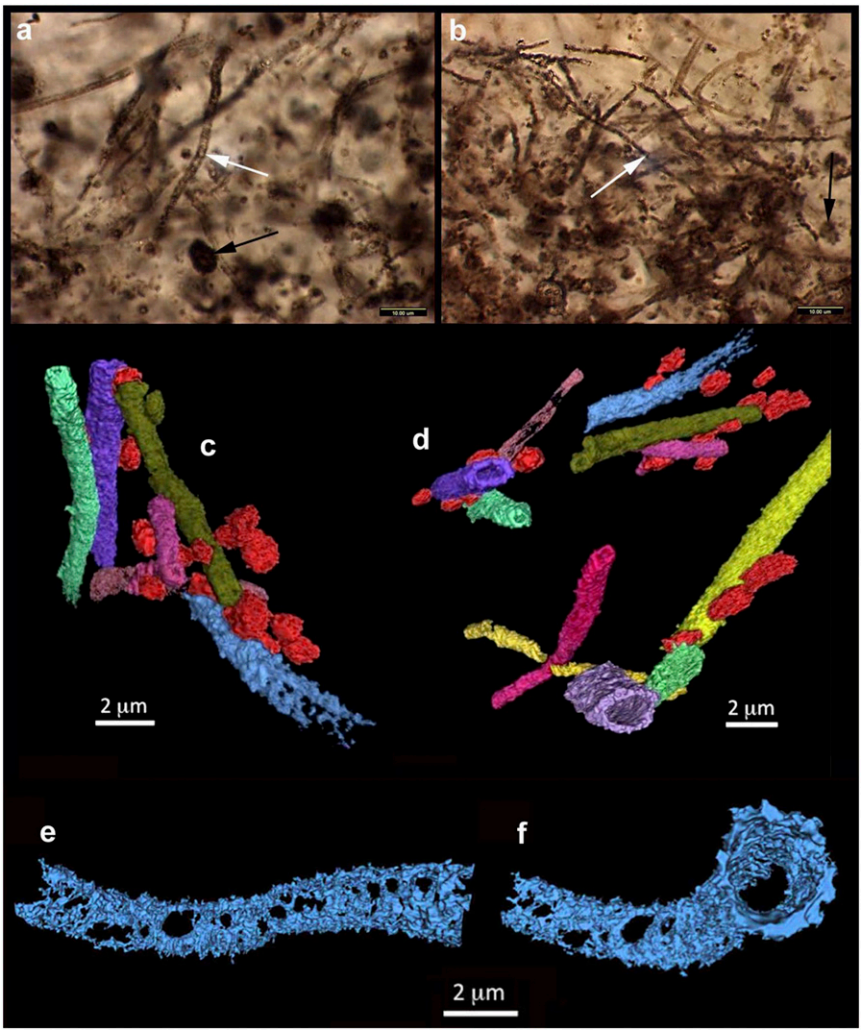

Fig. S2. Typical preservation of 1.88-Ga filamentous microfossil *Gunflintia* within the chert of the Gunflint Formation, Schreiber Beach, Ontario. (*A* and *B*) Optical images of a 30-µm thin section through a stromatolitic microbial mat, showing carbonaceous filaments of *Gunflintia* (white arrow points to examples with septate appearance) plus rounded vesicles of cyst-like *Huroniospora* (black arrows). (*C* and *D*) The 3D reconstructions from FIB-SEM sequential slicing of pyritized *Gunflintia* filaments (various colors) showing clusters of tubular sheaths bearing small epiphytic cells (orange/red). (*E* and *F*) The 3D reconstructions from FIB-SEM sequential slicing of a single, pseudoseptate carbonaceous *Gunflintia* filament, here interpreted as a microbial sheath affected by early decomposition and diagenetic silica growth (forming the rounded holes). *C–D* modified from ref. 1. *E–F* modified with permission from ref. 2.

1. Wacey D, et al. (2013) Nanoscale analysis of pyritized microfossils reveals differential heterotrophic consumption in the ~1.9-Ga Gunflint chert. *Proc Natl Acad Sci USA* 110(20): 8020–8024.
2. Wacey D, et al. (2012) Taphonomy of very ancient microfossils from the ~3400 Ma Strelley Pool Formation and ~1900 Ma Gunflint Formation: New insights using a focused ion beam. *Precambrian Res* 220-221:234–250.

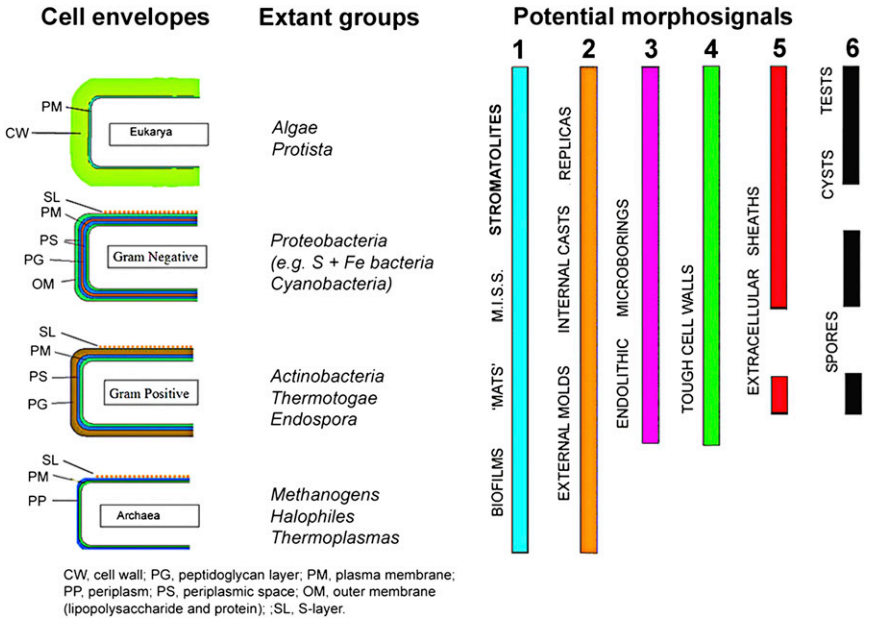

Fig. S3. Summary diagram illustrating some of the ways in which diverse microbial groups and/or their cellular envelopes might have been able to enter the early fossil record. At *Left,* four contrasting types of cell envelopes (adapted and extended from ref. 1), along with named extant groups that might be expected to leave geological signals (e.g., ref. 2). At *Right,* suggested some potential morphological signals that might have been left behind in the fossil record: 1, biolfims, microbial mats, MISS (microbially induced sedimentary structures), and stromatolites are all forms of organosedimentary structure that may leave distinctive signals (e.g., ref. 3); 2, external molds, internal casts, and replicas are mineral growths that may conserve some cellular information (e.g., refs. 4 and 1); 3, endolithic microborings are a form of microbial trace fossil that may leave morphological and geochemical clues, typically within carbonate rocks and volcanic glass (e.g., ref. 5); 4, tough cell walls include the thicker, stronger envelopes of bacteria and eukaryotic algae—their preservation tends to be rare; 5, extracellular sheaths consist of expolymers, often mucilaginous (rounded, tubular, amorphous), that help to protect the cells from physical or chemical damage and are not especially rare in the early fossil record; 6, spores, cysts, and tests here include those more resistant polymeric substances used to construct vesicles for protection or dispersal that may have a higher chance of preservation and retrieval in the fossil record (e.g., ref. 6).

1. Rickard D (2012) *Sulfidic Sediments and Sedimentary Rocks* (Elsevier, Amsterdam), 801 pp.
2. Konhauser KO (2006) *Introduction to Geomicrobiology* (Blackwell, Oxford).
3. Noffke N (2010) *Microbial Mats in Sandy Deposits from the Archean Era to Today* (Springer, Berlin).
4. Wacey D, et al. (2013) Nanoscale analysis of pyritized microfossils reveals differential heterotrophic consumption in the ~1.9-Ga Gunflint chert. *Proc Natl Acad Sci USA* 110(20): 8020–8024.
5. McLoughlin N, Brasier MD, Wacey D, Green OR, Perry RS (2007) On biogenicity criteria for endolithic microborings on early Earth and beyond. *Astrobiology* 7(1):10–26.
6. Armstrong HA, Brasier MD (2005) *Microfossils* (Blackwell, Oxford), 2nd Ed, 296 pp.

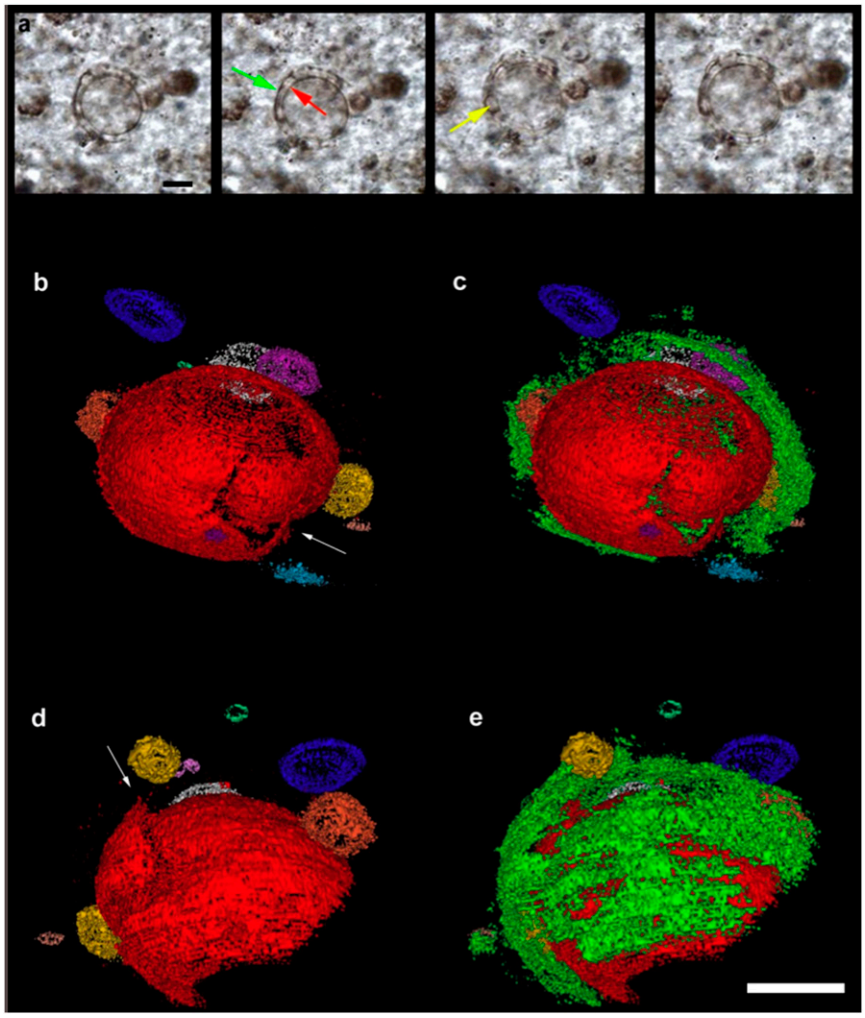

Fig. S4. Exceptional preservation and unique morphology within complex carbonaceous microfossil *Eosphaera tyleri* from the 1.88-Ga Gunflint chert at Schreiber Beach, Ontario. (*A*) Four optical images through a 30-μm thin section within nonstromatolitic fabric, at four levels of focus, showing the *Eosphaera* analyzed below and in Figs. 1 and 2, complete with the inner sphere (red arrow) and outer sphere (green arrow) plus rounded tubercles (yellow arrow) within the intervallar space. (*B*–*E*) The 3D reconstructions of the same *Eosphaera* specimen, using FIB-SEM sequential slicing. Note the thicker and more robust inner sphere (red) with linear rupture (beneath white arrow), thinner and more membranous outer sphere (green), and about 10 rounded cell-like tubercles (various colors including yellow), plus two external tubercles (e.g., dark blue). (*B* and *C*) Data set showing just the inner sphere (*B*) or both the inner and outer spheres (*C*), both viewed from the inside. (*D* and *E*) Complete reconstruction viewed laterally showing just the inner sphere (*D*) or both the inner and outer spheres (*E*). Measurements of the larger spherical structures are as follows: Maximum diameter of the outer sphere (green) is 30 μm; maximum diameter of the inner sphere (red) is 20 μm; thickness of the inner sphere membrane (red) is *ca*. 200 nm; and thickness of the outer sphere membrane (green) is less than 200 nm, but proved hard to measure because it is so fragmented. Measurement of small tubercles (various colors) are as follows. Large blue (external): elliptical, 5.5–7 μm across; large orange/brown: elliptical, 4.6–5.8 μm across; large white: slightly elliptical, 5.2–5.5 μm across; large pink/purple: spherical, 5.2 μm across; pale blue: vaguely circular, 5 μm across max but nature of object less certain; yellow far right: elliptical, 4.4–4.7 μm across; yellow at top: spherical, 3.4 μm across; small brown: spherical, 1.9 μm across; small pale green (external): spherical, 1.8 μm across; 2 × small pink: spherical, larger 1.5 μm across and smaller 1 μm across. (Scale bar, 10 μm.)

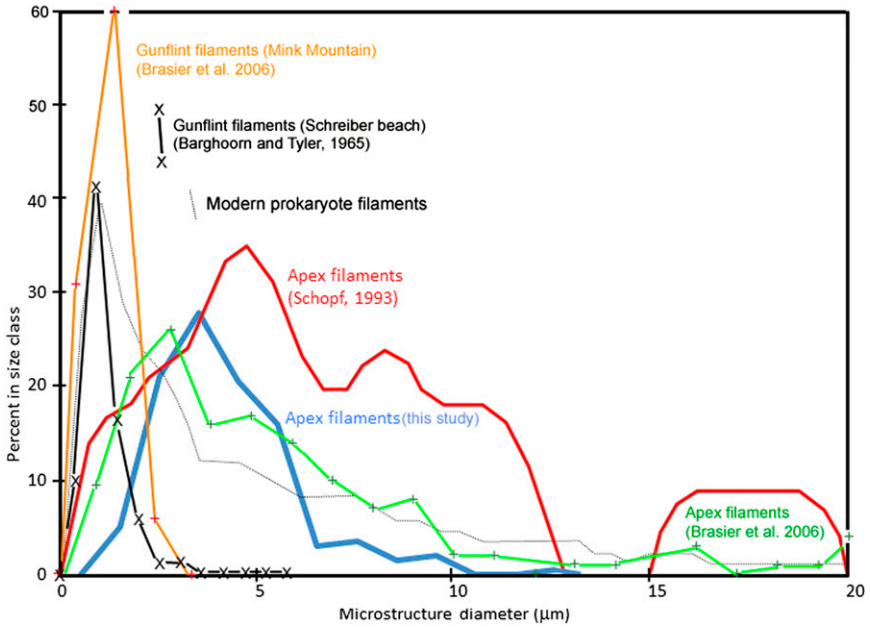

Fig. S5. Widths of filaments from sample CHIN-03 (blue) compared with previous data from the Apex chert (red and green), and compared with cell widths of modern bacteria (dotted line) and microfossils from the Gunflint Formation (black and gold). Additional data plotted from refs. 1, 2, and 3.

1. Barghoorn ES, Tyler SA (1965) Microorganisms from the Gunflint Chert. *Science* 147(3658):563–577.
2. Brasier M, McLoughlin N, Green O, Wacey D (2006) A fresh look at the fossil evidence for early Archaean cellular life. *Philos Trans R Soc Lond B Biol Sci* 361(1470):887–902.
3. Schopf JW (1993) Microfossils of the Early Archean Apex chert: New evidence of the antiquity of life. *Science* 260(5108):640–646.

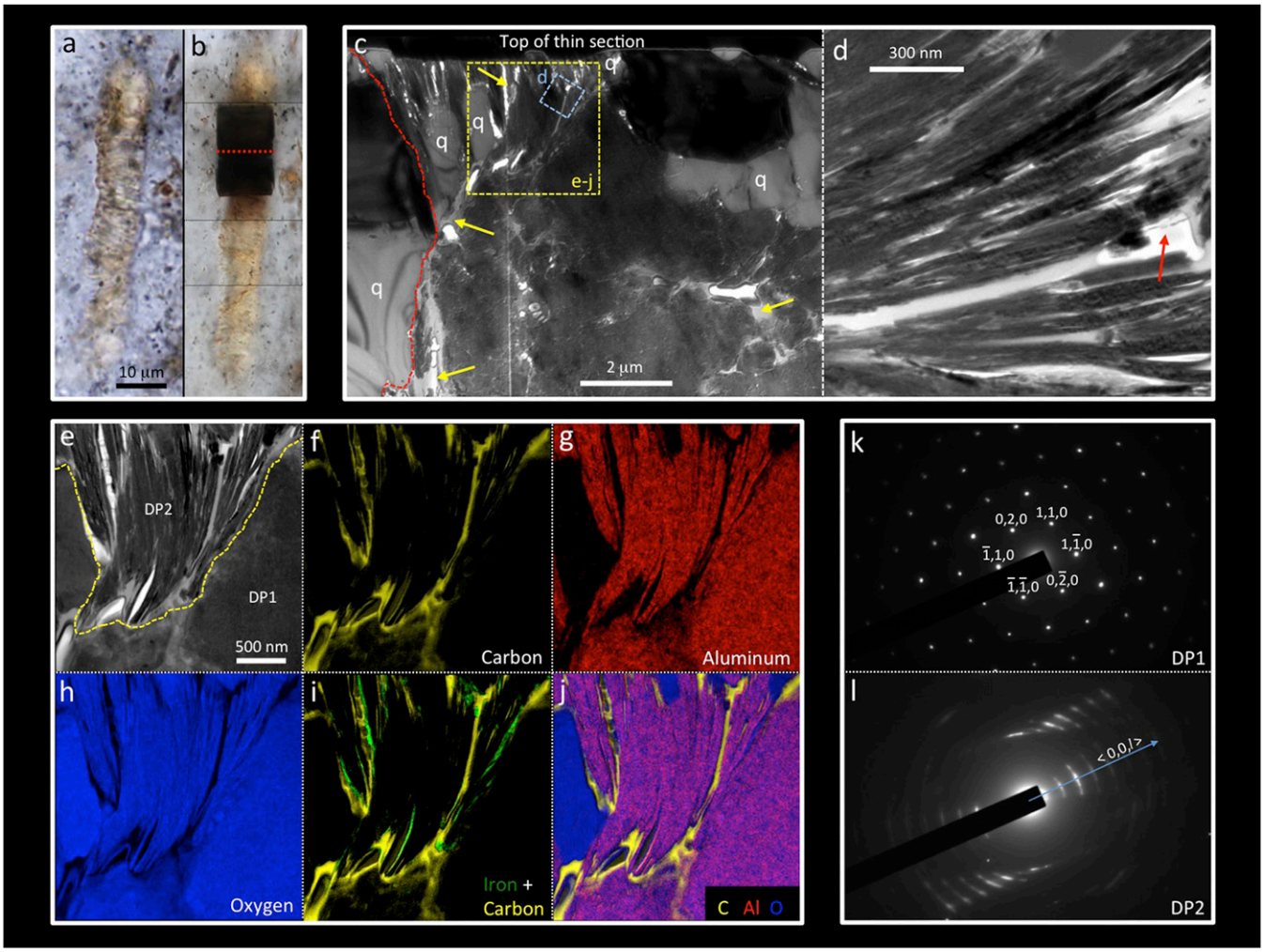

Fig. S6. Nanoscale structure and chemistry of a vermiform pseudofossil comparable to *Archaeoscillatoriopsis grandis* (1) from populations in the Apex chert dyke (microfossil site, sample CHIN 03). (*A* and *B*) Optical photomicrographs of *A. grandis* before and after extraction of an ultrathin wafer for analysis by TEM. Position of wafer indicated by red dashed line in *B*. Thin black lines in *B* separate images taken at different focal depths. (*C*) Bright-field TEM image showing an overview of the pseudofossil (left margin denoted by dashed red line) below the surface of the thin section. It comprises plate-like phyllosilicate grains (dark gray, spikey in cross section at top of image), minor quartz (q), and significant carbon (pale gray/white; four examples arrowed). (*D*) Bright-field TEM image of the blue-boxed area indicated in *C* showing the thin plate-like morphology of the phyllosilicates (dark gray) and the interleaving of carbon (light gray) between the phyllosilicate grains. Arrow points to a small hole within the carbon. (*E*) Bright-field TEM image and (*F*–*J*) false-color energy-filtered TEM elemental maps of the yellow-boxed region indicated in *C*. Carbon (yellow) is clearly interleaved between platy phyllosilicate grains (red) and shows no resemblance to cellular compartments. Minor iron (green) is also present, closely associated with carbon along many grain boundaries (*I*). This suggests that carbon and iron followed the same grain boundary conduits to enter the vicinity of the vermiform pseudofossil. The three-color overlay (*J*) most clearly demonstrates the distribution of quartz (blue), phyllosilicate (pink), and carbon (yellow) in this pseudofossil. (*K* and *L*) Selected area electron diffraction patterns from the regions of the TEM wafer indicated in *E*. DP1 is consistent with the [001] zone axis pattern from a 2:1 phyllosilicate. DP2 shows a pattern of ring arcs, representative of a set of closely aligned grains of a 2:1 phyllosilicate with the beam incident parallel to the {00l} plane.

1. Schopf JW (1993) Microfossils of the Early Archean Apex chert: New evidence of the antiquity of life. *Science* 260(5108):640–646.

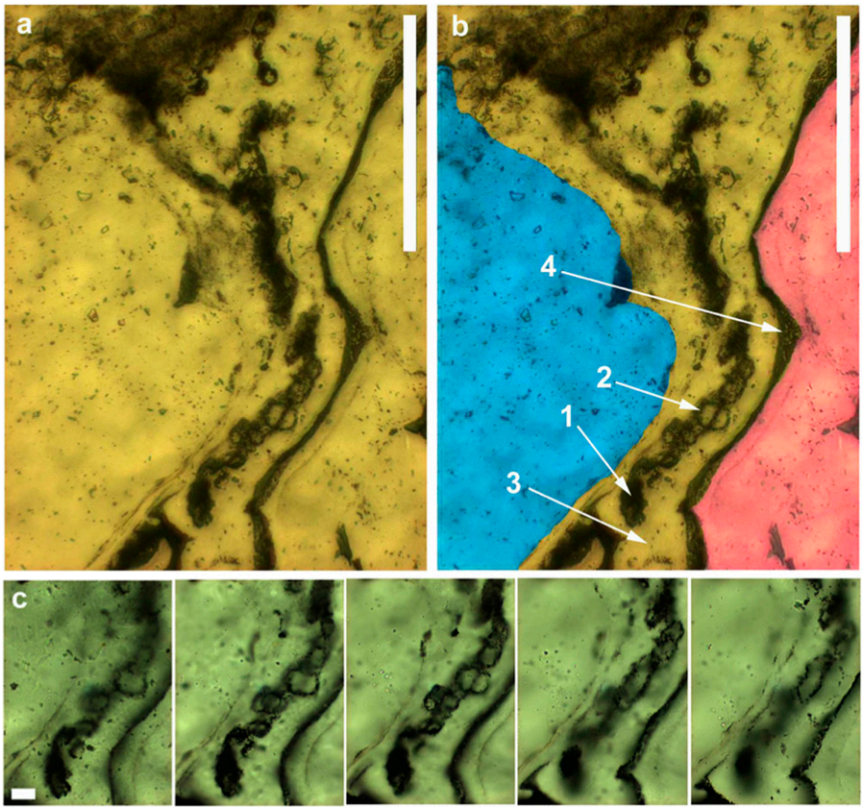

Fig. S7. Optical images of microfossil candidates preserved within dripstone-like chert fabrics of the 3.43-Ga Strelley Pool arenite, Western Australia. (*A* and *B*) Images showing the margins of a rounded sand grain of detrital quartz (highlighted in blue in *B*), coated with a multilayered veneer of chert (shown yellow in *B*) that contains filaments (1), made of from a chain of rounded, carbonaceous, cell-like structures (2). These carbonaceous structures are encased within cylindrical coatings (*ca*. 50 μm thick) of chert (3) that typically display carbon-coated botryoidal outer margins (4) as well as rounded terminations (see Fig. S9) consistent with a dripstone origin. The void was rapidly infilled with further layers of fine- to medium-grained quartz (shown pink in *B*). (*C*) Detail of the lower portion of *A*, showing five images taken at different focal depths which illustrate that these Strelley Pool filaments are constructed from a loosely arranged chain of rounded to elongate, carbonaceous, silica-filled cell-like structures. All images are plain polarized light micrographs from sample SPV3. [Scale bars, 100 μm (*A* and *B*) and 10 μm (*C*).]

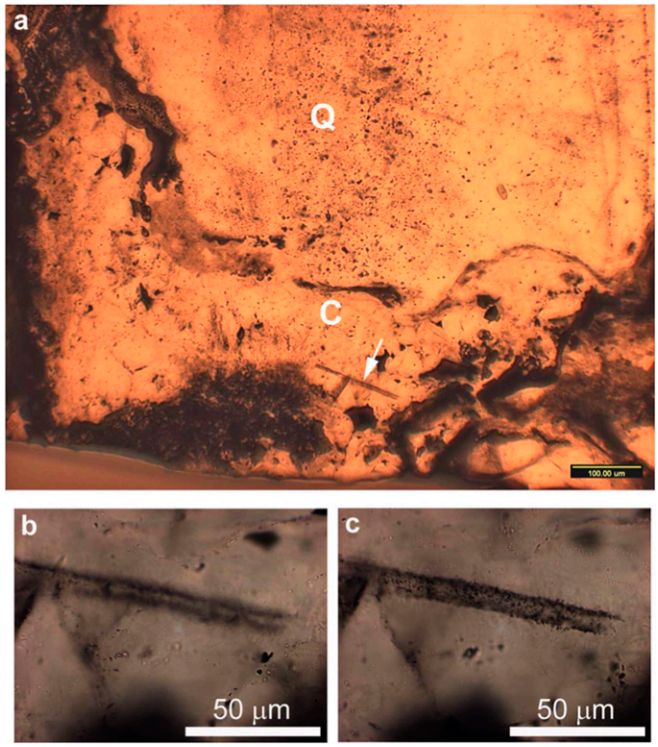

Fig. S8. Optical images of a sheath-like microfossil candidate preserved within dripstone-like chert fabrics of the 3.43-Ga Strelley Pool arenite, Western Australia. (*A*) A small cavity (C) formed beneath a quartz sand grain (Q) crossed by a distinct dark tube (white arrow) that takes the form of a hollow, carbonaceous sheath-like structure. (*B* and *C*) Detail of the structure, showing two images taken at different focal depths illustrating a hollow and silica-filled construction provided with a rounded cross section. All images are plain polarized light micrographs from sample SPV3.

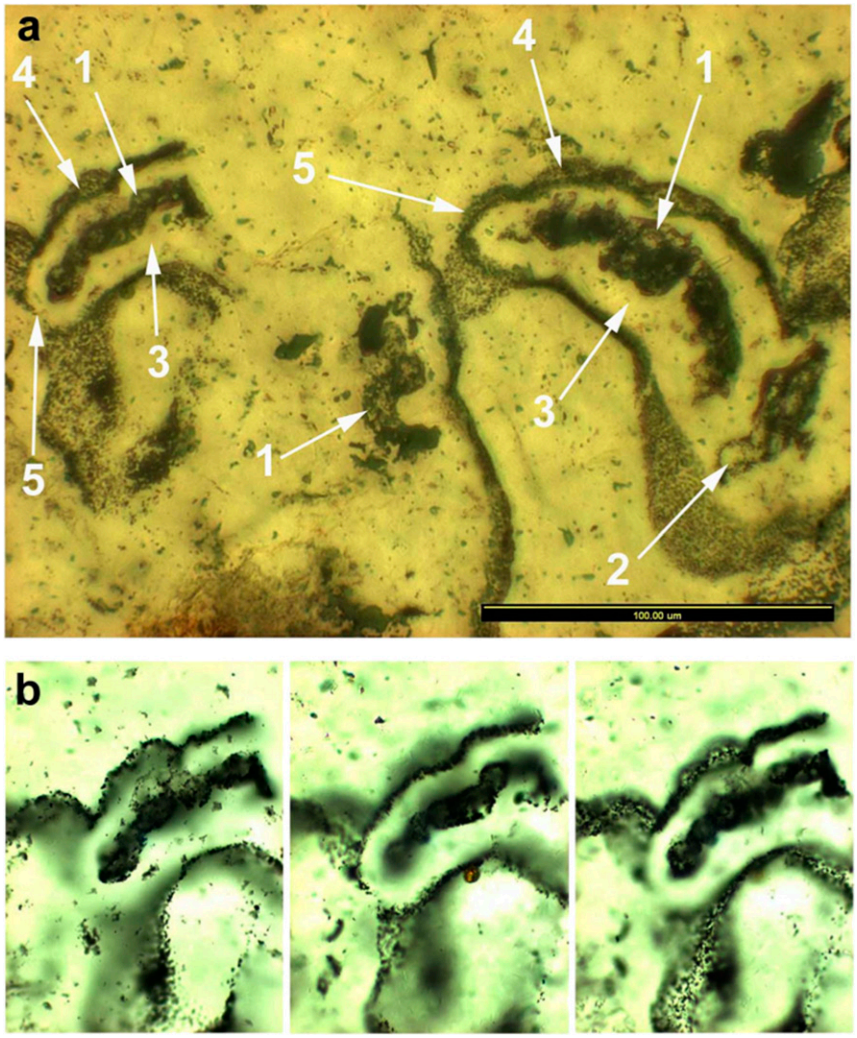

Fig. S9. Optical images of microfossil candidates preserved within dripstone-like chert fabrics of the 3.43-Ga Strelley Pool arenite, Western Australia. (*A*) A small cavity formed between quartz sand grains crossed by three distinct dark filaments (1), made of a chain of rounded, carbonaceous, cell-like structures (2). These carbonaceous structures are infilled and encased within cylindrical coatings (*ca*. 50 μm thick) of chert (3) that typically display carbon-coated botryoidal outer margins (4) as well as rounded terminations (5) consistent with a dripstone origin. (*B*) Detail of the left portion of *A*, showing three images taken at different focal depths which illustrate that these Strelley Pool filaments are constructed from a loosely arranged chain of rounded, carbonaceous, silica-filled cell-like structures. The microtexture of the cell-like structures is found to be different from that of the botryoidal outer coatings (see ref. 1). The former consists of continuous carbonaceous walls of approximately uniform thickness, while the latter consists of isolated nanoparticles of carbon arranged in zones of very variable thickness (see ref. 1). Future work will aim to determine if the botryoidal carbon is redistributed biological material or a completely different generation of abiotic carbon. All images are plain polarized light micrographs from sample SPV3. (Scale bar, 100 μm.)

1. Wacey D, et al. (2012) Taphonomy of very ancient microfossils from the ~3400 Ma Strelley Pool Formation and ~1900 Ma Gunflint Formation: New insights using a focused ion beam. *Precambrian Res* 220-221:234–250.

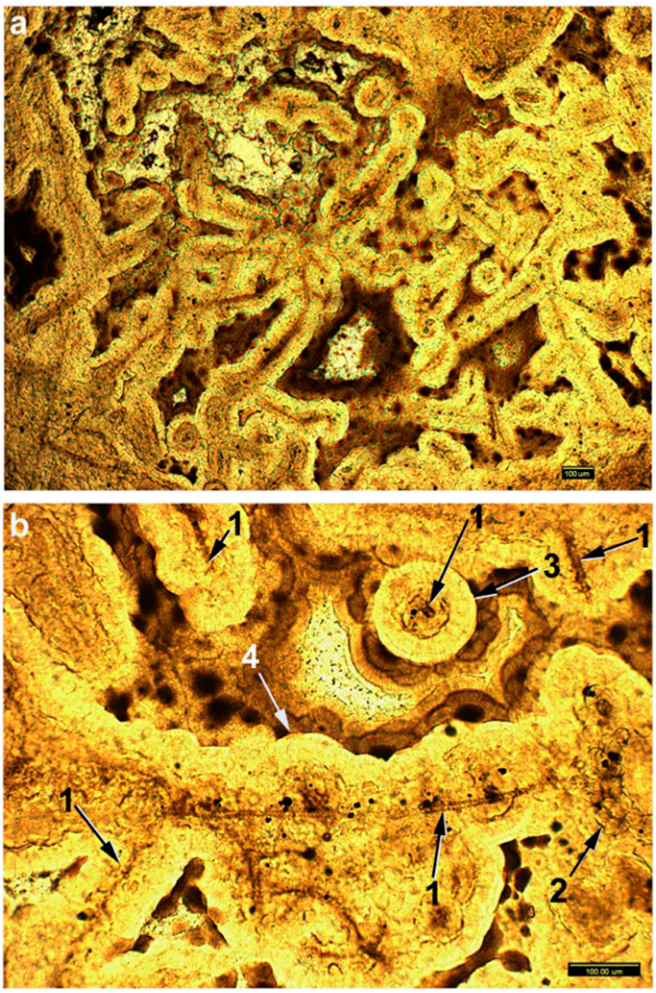

Fig. S10. Optical images of microfossils preserved within dripstone-like chert fabrics of the early Devonian Rhynie Chert, Aberdeenshire. (*A*) General field of view of a space between plant material that is crossed by dark hollow filaments (putative fungal hyphae), here infilled and encased within often carbon-coated cylindrical coatings (*ca*. 100 μm) of dripstone chert. (*B*) Detailed view of similar fabric showing longitudinal and transverse sections through probable fungal hyphae (1), and a coccoid cell cluster (2), both encased within cylinders of dripstone chert (3), provided with botryoidal outer margins (4). (Scale bar, 100 μm.)

Table S1. Distinguishing characters of Apex microfossil taxa that can also be observed in the new CHIN-03 material presented herein

Apex microfossil taxon	Distinguishing features	Examples herein
Archaeoscillatoriopsis grandis		Fig. 3 *G–I*
Medial cells	8–11.5 μm wide; disk-shaped	
Terminal cells	flat rounded or hemispheroidal	
Filament	not attenuated toward apices	
Archaeoscillatoriopsis disciformis		Fig. 3 *A–C*
Medial cells	3–5.5 μm wide; disk-shaped	
Terminal cells	hemispheroidal or globose	
Filament	may be attenuated toward apices	
Primaevifilum attenuatum		Fig. 3 *J–L*
Medial cells	4–12 μm wide; disk-shaped	
Terminal cells	flat rounded	
Filament	strikingly attenuated toward apices	
Primaevifilum laticellosum		Fig. 3 *M–O*
Medial cells	6–8.5 μm wide; short cylinders or quadrate	
Terminal cells	pillow shaped	
Filament	may show slight attenuation toward apices	
Primaevifilum conicoterminatum		Fig. 3 *P–R*
Medial cells	4–6 μm wide; disk-shaped or short cylinders	
Terminal cells	conical or blunt rounded	
Filament	attenuated toward apices	
Primaevifilum delicatum		
medial cells	1.8–3.2 μm wide; disk-shaped or short cylinders	Fig. 3 *D–F*
terminal cells	flat or flat rounded	
filament	not attenuated toward apices	
Primaevifilum minutum		
medial cells	1.2–2.1 μm wide; quadrate	not illustrated
terminal cells	flat rounded	
filament	not attenuated toward apices	
Primaevifilum amoenum		Fig. 3 *X–Z*
Medial cells	2–5 μm wide; quadrate or disk-shaped	
Terminal cells	hemispheroidal	
Filament	attenuated toward apices	

Characters are summarized from ref. 1, table 1. Examples of the remaining three Apex taxa—*Archaeotrichion septatum*, *Eoleptonema apex*, and *Archaeoscillatoriopsis maxima*—have not yet been observed in CHIN-03 material.

1. Schopf JW (1993) Microfossils of the Early Archean Apex chert: New evidence of the antiquity of life. *Science* 260(5108):640–646.

Table S2. Summary of observations suggested by us to point towards a biogenic origin for the Strelley Pool microfossils

Characteristics	Details
1. Biological behavior	The cell-like microstructures colonize the edges of grains and pore spaces in the manner of biofilms.
2. Biological morphology	The microfossil-like microstructures compare morphologically with forms of extant cell envelopes and sheaths.
3. Taphonomic decay	The microstructures exhibit taphonomic decay features comparable with those of younger biological assemblages including those from the 1.88-Ga Gunflint chert.
4. Fossil–mineral interaction	Interactions are inferred between the microstructures and associated fossilizing minerals: The silica appears to have nucleated on the candidate cell envelopes and grown away from them, as expected from modern settings and experiments.
5. Metabolism	Evidence for a plausible metabolic pathway, involving the fractionation of sulfur isotopes, is preserved in pyrite within and around the candidate cell envelopes.
6. Biochemistry	The microstructures are enriched in nitrogen that correlates well with the carbonaceous composition of the candidate cell envelopes.
7. Context	The context of the candidate cell envelopes is well understood. The geological setting is well-constrained and habitable. The morphology and metabolism of the candidate cells fit within the known evolutionary context.
8. Difference from cooccurring artifacts	Clear morphological differences are found between the candidate cells/sheaths and cooccurring botryoids/mineral coatings.
9. Distribution	The candidate microfossils are numerous and have frequency size distributions comparable with those of younger biological assemblages.

These lines of evidence are discussed in more detail in refs. 1 and 2.

1. Wacey D, et al. (2012) Taphonomy of very ancient microfossils from the ~3400 Ma Strelley Pool Formation and ~1900 Ma Gunflint Formation: New insights using a focused ion beam. *Precambrian Res* 220-221:234–250.
2. Wacey D, Kilburn MR, Saunders M, Cliff J, Brasier MD (2011) Microfossils of sulfur metabolizing cells in ~3.4 billion year old rocks of Western Australia. *Nat Geosci* 4:698–702.